A Physical–Statistical Approach to Match Passive Microwave Retrieval of Rainfall to Mediterranean Climatology

Luca Pulvirenti, Nazzareno Pierdicca, Frank Silvio Marzano, *Member, IEEE*, Paolo Castracane, and Giovanni d'Auria

***Abstract*—A physical–statistical approach to simulate cloud structures and their upward radiation over the Mediterranean is described. It aims to construct a synthetic database of microwave passive observations matching the climatological conditions of this geographical region. The synthetic database is conceived to train a Bayesian maximum *a posteriori* probability inversion scheme to retrieve precipitating cloud parameters from spaceborne microwave radiometric data. The initial microphysical *a priori* information on vertical profiles of cloud parameters is derived from a mesoscale cloud-resolving model. In order to complement information from cloud models and to match simulations to the conditions of the area of interest, a new approach is proposed. Climatological constraints over the Mediterranean are derived on a monthly basis from available radiosounding profiles, rain-gauge network measurements, and colocated METEOSAT infrared measurements. In order to introduce the actual surface background in the radiative-transfer simulations, a further constraint is represented by the monthly average and variance maps of surface emissivity derived from Special Sensor Microwave Imager (SSM/I) clear-air observations. A validation of the forward model is carried out by comparing a large set of brightness temperatures measured by the SSM/I with the synthetic cloud radiative database to asses its representativeness and range of variability. The marginal contribution of each constraint source, used in the matching process, is also evaluated. Finally, surface rain rates, retrieved from SSM/I data using the new synthetic database, are compared with colocated rain rates measured by a rain-gauge network along the Tiber River basin in Italy throughout 1995. This comparison is performed both for selected case studies and in a statistical way, discussing the major advantages and limitations of the proposed approach.**

***Index Terms*—Atmospheric remote sensing, clouds and precipitation, microwave radiative transfer, spaceborne microwave radiometry.**

I. Introduction

ATMOSPHERIC precipitation plays a crucial role in the earth's hydrological cycle on both small and large scales, being a key parameter to determine latent heat budget and land runoff equilibrium [1]. Its relevant impact on human and social activities is a continuous prompt to devise more and more accurate techniques for its quantitative monitoring. Rain-gauge networks and/or weather radars for rainfall retrieval have represented for years a means to map and estimate rainfall [2], [3]. However, their major limitation is relative to the fact that the entire globe cannot be uniformly and systematically covered, especially over the ocean.

In the past decades, the problem of remotely sensing precipitation has also been successfully addressed by spaceborne microwave radiometry (e.g., [4] and [5]). Starting from the mid-1970s, the launches of near-polar satellites with multifrequency radiometers and, more recently, the Special Sensor Microwave Imager (SSM/I) and the Tropical Rainfall Measuring Mission (TRMM) Microwave Imager (TMI) have represented milestones in exploiting this technique [6], [7]. Several authors have studied the sensitivity of brightness temperature (T_B) at different frequencies to liquid and iced hydrometeors in clouds, demonstrating the sensitivity of T_B to hydrometeor composition and distribution in a frequency-dependent way (e.g., [8]). The availability of a sufficiently large number of frequency channels is essential to get a quantitative prediction of rainfall, either over land or over sea. In this respect, the SSM/I does not support a low-frequency channel around 10 GHz as the TMI does, whereas this capability notably enhances rain retrieval accuracy over the ocean (e.g., see [9]). For operational applications, the main drawback of near-polar platforms, where microwave radiometers are currently installed, is the high revisit time (about 12 hours), a limitation that can be partially mitigated by the availability of an increasing number of satellites and by a multimission data integration approach [10].

Several inversion methods have been applied to extract rainfall rates from multifrequency radiometric images (e.g., [4], [5], and [10]–[16]). Most retrieval algorithms use linear, nonlinear, or iterative inversion techniques. They are aimed at providing, as a final product, the surface rain rate and/or the integrated parameters and/or the vertical profiles of cloud and precipitation hydrometeor contents. The development of the inversion scheme can be based either on an empirical or a physical approach. The difference between the two approaches stems from the fact that they can be trained by colocated ground-based and radiometric measurements or by one-dimensional or three-dimensional (3-D) cloud models coupled with microwave radiative-transfer schemes.

Manuscript received September 29, 2001; revised July 12, 2002. This work was supported in part by the Italian Space Agency (ASI), the Italian Ministry of Education, University and Research (MIUR), and the European project EURAINSAT.

L. Pulvirenti, N. Pierdicca, P. Castracane and G. d'Auria are with the Department of Electronic Engineering, University of Rome "La Sapienza," 00184 Rome, Italy (e-mail: pulvirenti@mail.die.uniroma1.it; nazzareno.pierdicca@uniroma1.it; castracane@mail.die.uniroma1.it; dauria@mail.die.uniroma1.it).

F. S. Marzano is with the Department of Electrical Engineering—Center of Excellence CETEMPS, University of L'Aquila, 67040 L'Aquila, Italy (e-mail: marzano@ing.univaq.it).

Digital Object Identifier 10.1109/TGRS.2002.803625

Nevertheless, several issues still remain open problems, particularly over land, as emphasized by validation experiments conceived to assess the accuracy of rainfall estimates [2], [3], [17]. With respect to empirical approaches, based exclusively on spaceborne and ground measurements, physical inversion techniques can take advantage of the various degrees of freedom offered by a forward radiative-transfer model based on the proper characterization of thermodynamic, geometrical, and dielectric parameters of the cloudy atmosphere (e.g., [5], [9], [11], and [17]). The model approach permits one to adapt individual parameters to specific conditions of the observed scenario and to the configuration of the considered microwave radiometer, without requiring new experimental campaigns. With respect to purely empirical approaches, this is an appealing feature that allows one to investigate new spaceborne passive instruments and advanced retrieval techniques by acting in a self-consistent simulation environment. As a drawback, model-based approaches always need to deal with the capability of the models themselves to represent the "real scenario" (atmosphere plus earth surface).

Since it is unfeasible to dispose of a large number of cloud-resolving model simulations adapted to specific geophysical and climatological conditions, the cloud radiative model parameters are sometimes modified to better tune the brightness temperature simulations with spaceborne measurements (e.g., see [9] and [17]). Moreover, cloud models are not free of errors: comparisons among the most established ones have shown a large degree of variability both for case studies and long time analyses (e.g., see [18]). We believe that this is a crucial point with a model-based retrieval method: the use of independent sources of cloud information can strongly improve the representativeness of the simulations for specific local geographical and climatogical conditions. The matching of the numerical simulations (i.e., of the synthetic clouds as well as their upward microwave radiation) can be achieved by exploiting all available ancillary information in order to characterize both the microphysical and radiative properties of cloud systems. Ground measurements, provided by rain-gauge networks, meteorological stations, and radiosounding balloons, as well as remote sensing data coming from other meteorological satellites (e.g., visible–infrared radiometers), can be pieces of this mosaic. The matching procedure should determine an overall statistical agreement between numerical simulations and measurements whose evaluation can be quantified in terms of mean values, variances, and correlations.

In previous works, in order to generate a precipitating cloud database, we resorted to the numerical outputs of a cloud-resolving mesoscale model with an explicit detailed microphysics. We considered a 3-D time-dependent cloud mesoscale model [4] to derive statistical characteristics of cloud hydrometeor contents, according to the standard meteorological classification into genera [14], [19]. This statistical information was extracted to randomly generate a database of cloud structures by using a Monte Carlo approach. The major limitation of the adopted approach has originated from the availability of only one cloud model simulation, referred to as a tropical convective storm over land. The application of this cloud radiative database to mid-latitude rainfall events was necessarily deficient in many respects (e.g., vertical development of cloud genera is strongly dependent on seasonal freezing level). As mentioned before, this is a situation very often encountered when adopting a model-based approach. In fact, cloud-resolving mesoscale models are not generally run operationally, while on the other hand general circulation models for weather forecasting are not suitable for these applications, since they generally lack a detailed microphysical characterization, which is essential for radiative-transfer simulations [18].

In this paper, we substantially extend the mentioned works by proposing a new physical–statistical approach to adapt the training database to the empirical evidence provided by complementary sources of meteorological data. The work is devoted to the simulation of SSM/I observations and rain retrieval over the Mediterranean area, but the methodology is easily extensible to other regions. Microphysical *a priori* knowledge and climatological constraints are derived from a joint analysis of mesoscale cloud models, available radiosounding profiles, rain-gauge network measurements, SSM/I data over the Mediterranean region, and colocated METEOSAT infrared measurements. Monthly maps of surface emissivity at SSM/I frequencies are also derived to introduce in the radiative model the actual surface boundary conditions. An assessment of the results is carried out by comparing a large set of SSM/I observations with the synthetic database of brightness temperatures. The marginal contribution of each source of meteorological information, utilized in the process of matching simulations with measurements, is also evaluated. Retrievals of surface rain rate, derived from SSM/I data using the new synthetic database as a training set, are compared with rain rates measured by a rain-gauge network over the Tiber River basin in central Italy during 1995. This comparison is performed both for selected case studies and in a statistical way, in order to assess advantages as well as limitations of the overall approach.

II. Physical–Statistical Matching

According to the physical approach, as opposed to the empirical one, the problem of retrieving cloud properties from spaceborne radiometric data is separated into cloud modeling and radiative modeling steps. As illustrated in previous works, the numerical outputs of a 3-D time-dependent cloud-resolving mesoscale model, named University of Wisconsin—Non-hydrostatic Modeling System (UW-NMS), have been used as a starting point to statistically generate the dataset of cloud vertical structures [14], [15], [19]. The UW-NMS model, whose validity has been recognized by several authors in the same application framework, is capable of explicitly describing the vertical distribution of four species of hydrometeors (i.e., cloud droplets, rain drops, graupel particles, and ice particles) [4]. From the original vertical resolution of about 0.5 km, which determines 42 altitude levels, the number of cloud layers has been reduced to at most seven [9], [14]. The cloud vertical structures have been classified into classes (i.e., genera and species) following the World Meteorological Organization nomenclature, i.e., cumulonimbus (Cb), cumulonimbus with incus (Cbi), cumulus (Cu), cumulus congestus (Cuc), altocumulus (Ac), altostratus (As), nimbostratus (Ns), stratus (St), and cirrus (Ci) [19]. Each cloud is defined by a vector $\mathbf{g} = [g_1, g_2, \ldots, g_D]$ whose elements g_l (with $l = 1, 2, \ldots, D$)

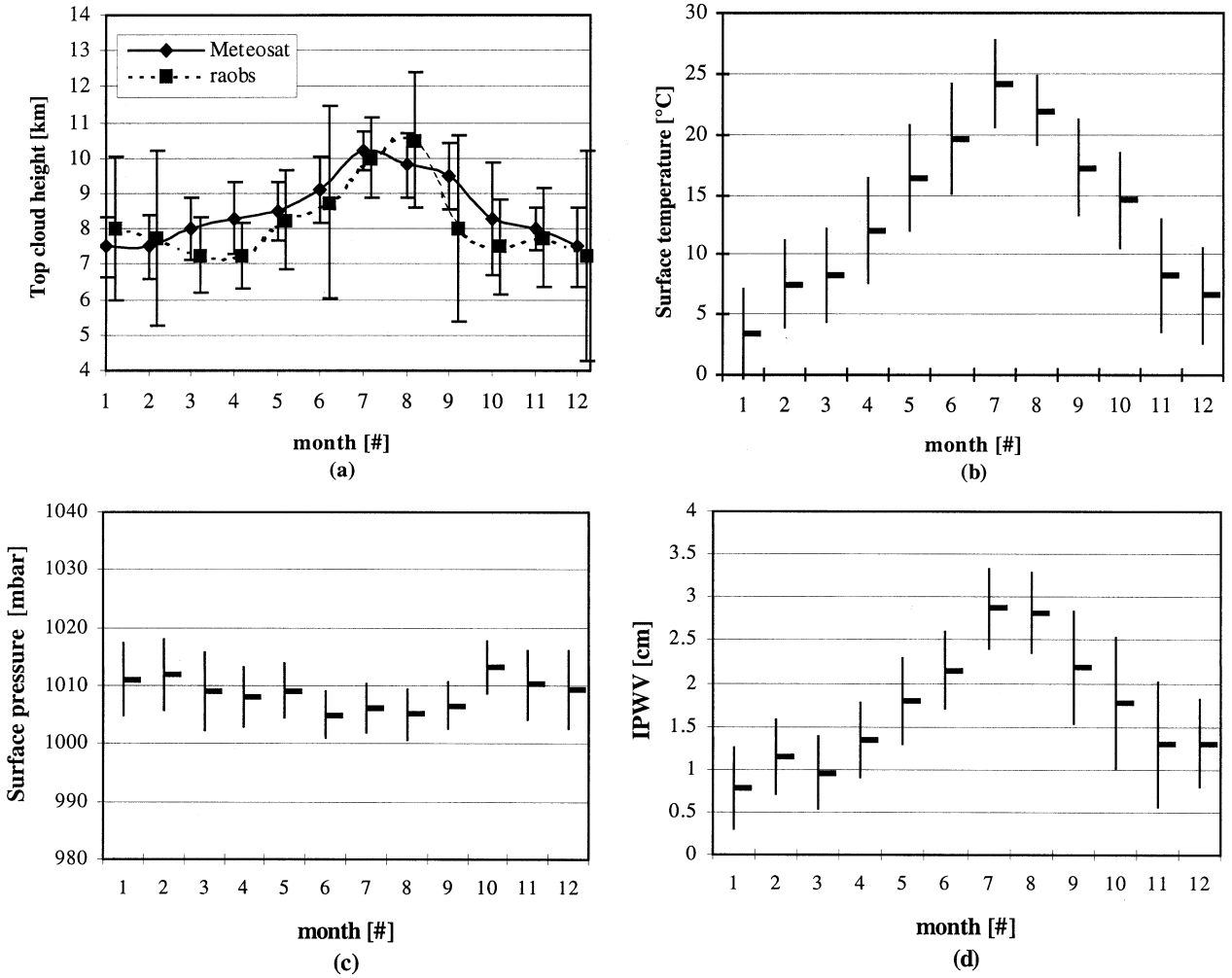

Fig. 1. Annual variation of top cloud maximum height, surface temperature, surface pressure, and the integrated precipitable water vapor as a function of the month, derived from radiosoundings in 1995. Cloud height is also derived from METEOSAT. Mean values as well as the ± 1 standard deviation intervals are reported.

are the equivalent water contents of the various hydrometeors; its dimension D can at most be 28 (i.e., seven layers by four hydrometeors). For the purpose of enlarging the database by using a Monte Carlo statistical generation, the vector $\mathbf{g}$ has been considered random with a Gaussian distribution within each cloud class i ($i = 1, \ldots, N_c$ with $N_c = 9$ here). Denoting with angle brackets the expected value, the ith cloud class has been characterized by means of the mean profile $\mathbf{m}_i = \langle \mathbf{g} \rangle$, the covariance matrix $\mathbf{C}_i = \langle (\mathbf{g} - \mathbf{m}_i)^T (\mathbf{g} - \mathbf{m}_i) \rangle$ (where superscript "T" indicates transposition), and the altitude of the layer boundaries $\mathbf{h}_i = [h_{1,i}, \ldots h_{t,i}, \ldots, h_{T,i}]$ ($t = 1, \ldots, T$ with $T = 7$) [14], [19]. A correlation matrix $\mathbf{R}_i$ can also be introduced for each class i, whose generic element $r_{jk,i}$ is given by

$$r_{jk,i} = \frac{c_{jk,i}}{\sqrt{c_{jj,i}}\sqrt{c_{kk,i}}} = \frac{c_{jk,i}}{\sigma_{j,i}\sigma_{k,i}}, \qquad j,k = 1, \ldots, D \quad (1)$$

where $c_{jk,i}$ is an element of the covariance matrix $\mathbf{C}_i$, and $\sigma_{k,i}$ is the standard deviation of hydrometeor content g_k within class i. Once $\mathbf{m}_i$, $\mathbf{C}_i$, and $\mathbf{h}_i$ are known, an arbitrarily large number of cloud structures can be statistically generated and their upward brightness temperatures (T_B) subsequently computed through the radiative model, using a plane parallel approximation.

The impact of some assumptions has been carefully evaluated in previous papers. For example, the choice of seven layers at most, as well as the number of generated clouds, is the result of a compromise between the requirement of generating a representative cloud database and avoiding computational complexity. In this tradeoff, it has been considered that the resolution (i.e., "density") of the synthetic database in the T_B domain is limited by the radiometric resolution of current spaceborne radiometers (in the order of 1 K) [14]. Other major concerns to be pointed out are the following:

1) characterization of cloud structures and parameters by using only a UW-NMS simulation of a summer convective storm that occurred in a tropical area;
2) discrepancy between environmental conditions of the UW-NMS numerical simulation with respect to local climatology in terms of both meteorological variables (i.e., temperature, humidity, and pressure) and rainfall amount;
3) uncertainty about microwave emissivity of sea and, especially, of land surfaces;
4) spatial inhomogeneity of cloud structures within the radiometric ground field of view.

The next paragraphs describe the approach we are proposing here to complement information from cloud-resolving models with a combined dataset of real measurements, generally available from operational services. This information, collected for the entire year 1995, consists of

1) SSM/I data over the western Mediterranean area, mainly from the F11 platform;
2) colocated METEOSAT infrared data over the same area;
3) radiosounding observations (RAOBs) over Italy (five stations) in the morning and late afternoon (which correspond approximately to F11 passes over Italy);
4) meteorological profiles derived from National Center for Environmental Prediction (NCEP) analyses;
5) rain-gauge network data over the Tiber River basin in central Italy, available every 30 min.

This dataset has been gathered for the sake of adjusting all the parameters that define every cloud class, namely $\mathbf{m}_i$, $\mathbf{C}_i$, and $\mathbf{h}_i$, as well as the radiative boundary condition due to the emissivity of the surface plus pressure, temperature, and humidity profiles.

Time and space distances among the various information sources are resumed hereafter:

— $\pm$15 min and about 10 km (half SSM/I pixel) between Meteosat and SSM/I data;
— from 50 km up to 600 km between the main area of interest (i.e., Tiber River basin) and RAOB stations;
— $\pm$15 min between available Meteosat image and RAOB launch time;
— $\pm$15 min and about 10 km (half SSM/I pixel) between rain-gauge and SSM/I data.

Note that, when deriving statistical parameters to perform the proposed physical–statistical matching, colocation of *in situ* data and spaceborne radiometer overpasses in space and time is not strictly required. An accurate colocation is only necessary when performing rain rate retrieval validation, as carried out in Section III.

A. Cloud Database Matching

Clear-air conditions represent a sort of background where cloud hydrometeors are embedded. If not properly described, mismatched clear-air meteorological profiles can produce a bias in the simulated brightness temperatures with respect to measurements.

In order to identify a regional clear-air climatology, RAOB profiles collected by five Italian stations throughout 1995 have been used. For the purpose of taking into account the seasonal variability, the monthly statistics of the main atmospheric parameters have been derived. Mean and standard deviation have been computed for the surface values of temperature T_s (i.e., m_T and σ_T), pressure p_s (i.e., m_p and σ_p), and water vapor density ρ_s (i.e., m_ρ and σ_ρ). Moreover, temperature lapse rate a, vapor density, and pressure scale height (i.e., H_ρ and H_p, respectively) have been evaluated on a monthly basis by fitting RAOB vertical profiles by a linear function for temperature and by an exponential function for pressure and water vapor. The modeled vertical profiles of temperature $T(z)$, pressure $p(z)$, and water vapor density $\rho(z)$ as a function of the altitude z can be written as follows:

$$T(z) = T_s + az \quad p(z) = p_s e^{-z/H_p} \quad \rho(z) = \rho_s e^{-z/H_\rho}. \quad (2)$$

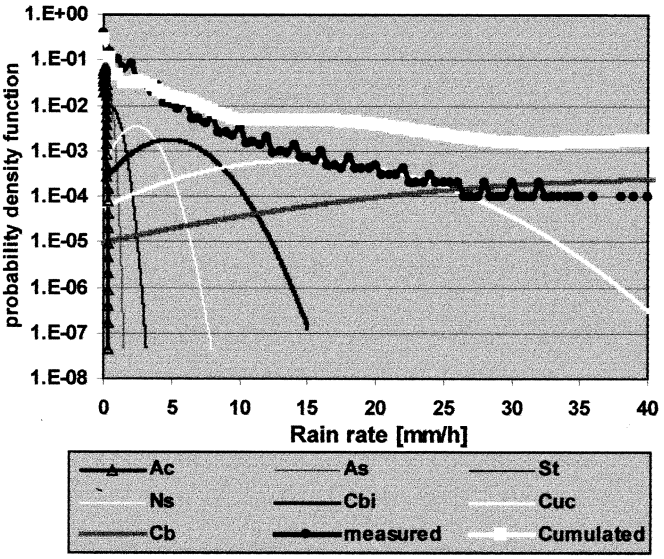

Fig. 2. Histograms of rain intensity measured by the rain-gauge network in central Italy compared with those derived from the statistically generated clouds. The histograms of simulated clouds are shown separately for each cloud class and for the total ensemble of classes (cumulated).

In the statistical generation of cloud structures, all meteorological surface parameters have been randomized in order to take into account the local unknown variability and the perturbation due to rainfall presence. The values at the surface (i.e., T_s, p_s, and ρ_s) have been statistically generated as Gaussian random variables with mean and standard deviation (i.e., m_T, σ_T, m_p, σ_p, m_ρ, and σ_ρ) estimated from all available RAOBs for each month. On the contrary, a, H_p, and H_ρ have been imposed as constant values for each month, as derived by best fitting the same RAOB profiles.

An important consequence of matching temperature profiles, besides a significant effect on gaseous absorption coefficients, was to determine more veritable altitudes of the freezing and glaciation levels of each cloud. These levels are used in the simulation to adjust the presence and absence of ice and liquid hydrometeors in order to ensure a microphysical consistency, as explained in [19].

Regarding the geometry of the cloud, a statistical evaluation of cloud-top height (corresponding to the cumulonimbus top height $h_{T,\mathrm{Cb}}$ in the primary database furnished by the UW-NMS model) has been carried out also on a monthly basis. The method is founded on the assumption that a cloud is detected if the relative humidity (RH) is beyond a given threshold (a value of 0.9 has been adopted here). For each RAOB profile, altitudes corresponding to RH values exceeding the threshold for increasing z identifies the bottom altitude h_B of a cloud, while the opposite condition identifies the top altitude h_T. Monthly histograms of the top altitude h_T have been computed, thus estimating $p(h_T)$, which is the probability density function (pdf) of h_T. The monthly cloud maximum height (i.e., cumulonimbus top height $h_{T,\mathrm{Cb}}$) has

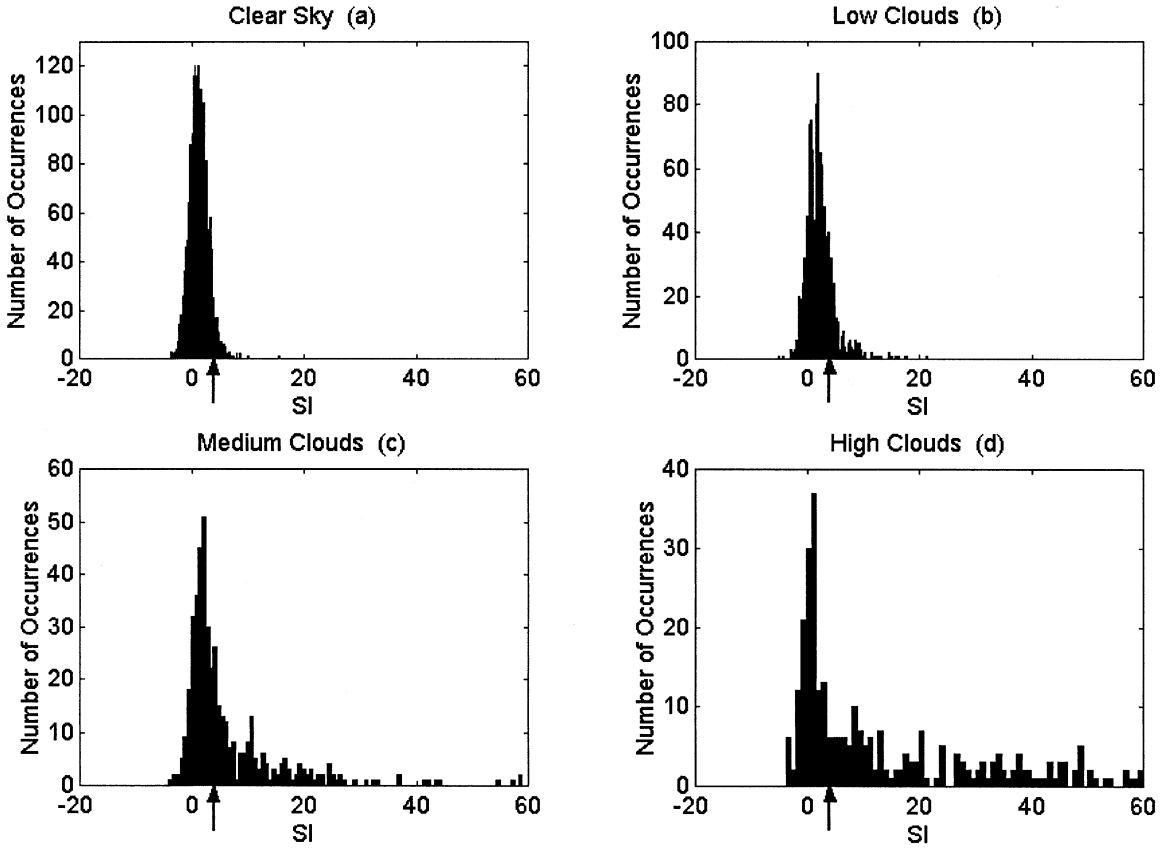

Fig. 3. Histograms of SI values relative to the four different classes derived from METEOSAT colocated infrared pixels in January 1995. The SI threshold able to identify pixels without scattering processes is also indicated in the figure by an arrow.

been inferred from the highest value below which 95% of the whole histogram area occurs, i.e., by imposing the following condition:

$$\int_0^{\hat{h}_{T,\mathrm{Cb}}} p\left(h_T\right) dh_T = 0.95. \tag{3}$$

The choice of 95%, instead of 100% (highest occurred value), has been adopted to remove possible blunders. In order to verify these estimates, we have evaluated the same quantity from METEOSAT images using the radiance R_{IR} measured in the thermal-infrared (TIR) channel converted into brightness temperature T_{IR} (i.e., black-body equivalent temperature). The monthly histograms of T_{IR} have thus given an estimate of pdf $p(T_{\mathrm{IR}})$, from which the minimum TIR temperature $T_{\mathrm{IR}m}$ (corresponding to the highest clouds) has been derived, as in (3), by the following condition:

$$\int_{T_{\mathrm{IR}m}}^{0} p\left(T_{\mathrm{IR}}\right) dT_{\mathrm{IR}} = 0.95. \tag{4}$$

In order to relate $T_{\mathrm{IR}m}$ to the cloud-top height, we have adopted a very simple approach. Since the cluster of the surface radiances (corresponding to cloud-free land and sea) is easily identified in the TIR histogram, its mean value has been computed to determine the surface radiance $R_{\mathrm{IR}s}$ and consequently the surface TIR temperature $T_{\mathrm{IR}s}$. The difference between these quantities, converted into altitude values by means of the monthly temperature lapse rate a, has been used to derive another estimate of the cloud maximum height. Analytically, this estimate of $h_{T,\mathrm{Cb}}$ is given by the following relation:

$$\hat{h}_{T,\mathrm{Cb}} = \frac{T_{\mathrm{IR}s} - T_{\mathrm{IR}m}}{a}. \tag{5}$$

The use of estimated cloud-top heights, derived by means of both (3) and (5), has allowed us to "compress" on a monthly basis the original vertical structures provided by the outputs of the UW-NMS model. To this aim, we have devided the vectors $\mathbf{h}_i$ of each cloud class, derived from the UW-NMS outputs as explained in [14], by the ratio between level $h_{T,\mathrm{Cb}}$ from UW-NMS outputs and $\hat{h}_{T,\mathrm{Cb}}$. One of the most important effects of matching the cloud-top height according to experimental data has been to produce lower mid-latitude clouds that are likely to take place in the Mediterranean region, in contrast with the UW-NMS outputs having the vertical development characteristics of tropical latitudes (e.g., original cumulonimbus extended up to 15 km).

Fig. 1 shows the annual variation of the most relevant meteorological parameters derived as explained above, presented as mean values plus and minus one standard deviation. Fig. 1(a) shows both the annual variation of the cloud maximum altitude computed from RAOBs and METEOSAT. A generally good agreement between the two different methods of evaluation is revealed so that we have finally considered the average of estimates from (3) and (5). The surface temperature in Fig. 1(b) and the integrated precipitable water vapor (IPWV) in Fig. 1(d) show an evident seasonal course. Note that the surface pres-

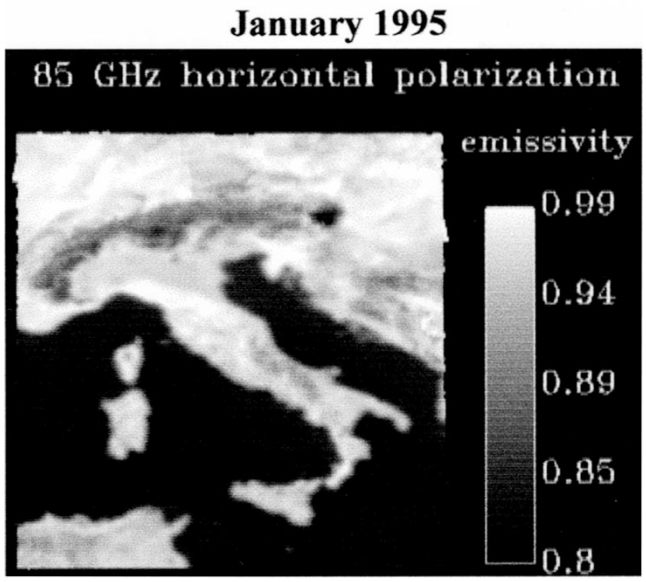

(a)

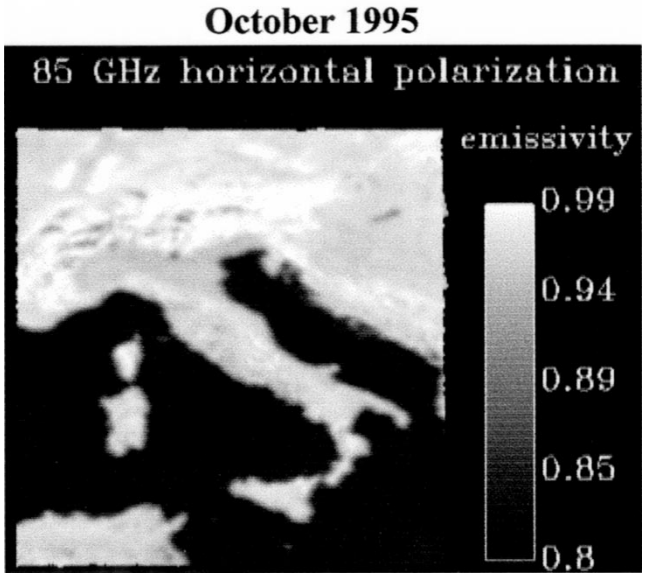

(b)

Fig. 4. Maps of the mean value of the 85-GHz surface emissivity (horizontal polarization) for (a) January 1995 and (b) October 1995.

sures shown in Fig. 1(c) are relative to the first radiosounding level, ranging from 3–104 m above sea level, depending on the RAOB station. The temperature lapse rate has been found in the range 6.6–7.1 K/km, the pressure scale height in the range from 7.4–8.0 km, and the water vapor scale height from 1.7–2.3 km.

For the purpose of preserving the original microphysics of the assumed cloud model, the correlation matrix $\mathbf{R}_i$ of hydrometeor contents initially derived from UW-NMS model has been adopted, as already done in [14], [15], and [19]. Unfortunately, the matching process cannot rely on adequate and extensive reference data concerning hydrometeor content distributions to be able to adapt mean values $\mathbf{m}_i$ and variances $\sigma^2_{k,i}$ to the climatological conditions of the Mediterranean area. In this study, the only information available for this purpose has consisted of rain-gauge network data over the Tiber River basin, collected for several years (from 1992 to 1997). We have used this information considering that the histograms of surface rain rate generated by the synthetic cloud structures of the database should have matched those measured by the rain-gauge network. The surface rain rate is related to hydrometer content $\mathbf{g}$ and, in particular, to the rain drop content in the first layer (element g_1), through the raindrop fall speed and size distribution [8].

A probability matching procedure has been applied to reproduce the measured rain rate statistics. To generate consistent cloud structures, a *scaling factor* has been applied to both mean vector $\mathbf{m}_i$ and standard deviation $\sigma_{k,i} (k = 1, \ldots, D)$ of the hydrometeor content $\mathbf{g}$. Note that standard deviation $\sigma_{i,k}$ and mean values m_k, derived by the UW-NMS outputs, are always fairly proportional for each cloud class and that this property has been preserved by the probability matching procedure. In formulas, let us assume RR is the rain rate and that $p_i(\mathrm{RR}; \mathbf{m}_i)$ is its pdf for cloud structures characterized by the hydrometeor mean vector $\mathbf{m}_i$ and belonging to the ith class. If $p_m(\mathrm{RR})$ is the pdf of RR estimated by computing the histogram of rain-gauge measurements, the probability matching consists in finding the scale factor α that minimizes the following functional:

$$\int_0^\infty \left[N_c p_m(\mathrm{RR}) - \sum_{i=1}^{N_c} p_i(\alpha \mathbf{m}_i, \mathrm{RR}) \right]^2 d\mathrm{RR} = \min . \quad (6)$$

The application of (6) to the available synthetic cloud database has revealed that a scaling (reduction) factor α of about 0.5 is needed to reproduce the measured rain rate statistics. Fig. 2 shows the histogram of rain rates in each simulated cloud genera, the total sample (all genera) histogram, and the experimental one. The factor α certainly accounts for many different causes that cannot be individually quantified because of the empirical nature of the implemented matching procedure. The original spatial resolution of the UW-NMS model as well as the time accumulation of the reference rain-gauge network should play the major role in determining its magnitude [4].

It is worth noting that the hypothesis of a Gaussian distribution of random vector $\mathbf{g}$ in each class does not contradict the usual assumption of log-normal distribution for rain. Indeed, the superposition of several cloud classes, having standard deviation fairly proportional to their mean, makes the total sample of simulated rainfall rates follow a distribution that is fairly similar to the log-normal one, as can be appreciated in Fig. 2. A χ-square statistical test on the total sample distribution of RR in the matched cloud database confirms its log-normal distribution with a 95% confidence interval.

B. Radiative Signature Matching

In order to associate a vector of brightness temperatures to each cloud structure, a plane-parallel radiative-transfer model, based on the fast and fairly accurate Eddington solution, has been applied [15], [19]. Within the radiative-transfer model, it is essential to constrain the surface emissivity in a fairly realistic way, since it influences the observations of a spaceborne radiometer, especially at low frequencies.

Once again, surface emissivity properties have been imposed in a statistical manner within the synthetic database, instead

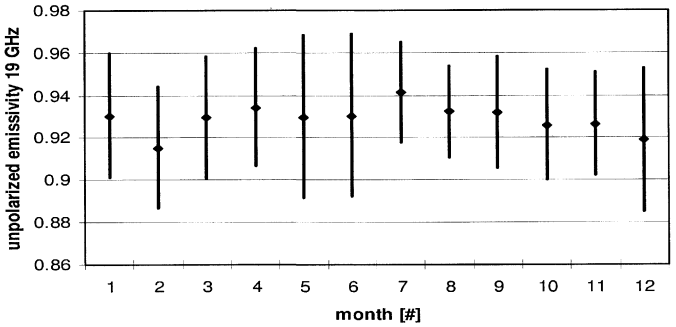

(a)

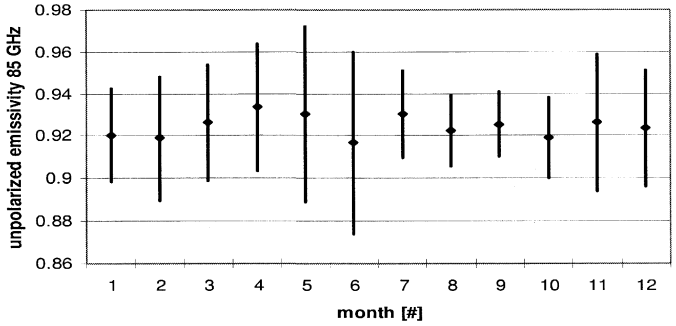

(b)

Fig. 5. Annual variation of mean value and standard deviation at (a) 19 GHz and (b) 85 GHz of the unpolarized emissivity (the average of vertical and horizontal polarizations) over central Italy.

of attempting to know the background emissivity when retrieving rainfall. In other words, values of frequency-dependent emissivity have been randomly generated to account for both temporal and spatial variability. We have assumed a Gaussian distribution for the multifrequency emissivity vector $\mathbf{e}_s$, whose mean vector $\mathbf{m}_e$ and covariance matrix $\mathbf{C}_e$ have been estimated on a monthly base by means of a historical archive of emissivity retrievals. For this purpose, SSM/I data related to nonprecipitating conditions have been used. In fact, the atmospheric microwave scattering being negligible, it is possible to solve the radiative-transfer equation for the surface emissivity e_s as follows [20]:

$$e_s = \frac{T_B - \left[T_{\mathrm{mrDN}} e^{-\tau/\mu} + T_{\mathrm{mrUP}}\right]\left[1 - e^{-\tau/\mu}\right]}{\left[T_s - T_{\mathrm{mrDN}}\left(1 - e^{-\tau/\mu}\right)\right] e^{-\tau/\mu}} \quad (7)$$

where T_s is the physical surface temperature, τ the atmospheric optical thickness, μ the cosine of the observation angle, and T_{mrUP} and T_{mrDN} the mean radiative temperatures for upward and downward radiometric observations, respectively. Indeed, through (7) a sort of "equivalent emissivity" or "composite emissivity" is estimated due to the large field of view of microwave channels at ground (from several up to tens of kilometers). Nevertheless, it represents what the radiometer is actually observing, consistent with its spatial and frequency resolution.

The absence of precipitation (and thus scattering) has been assessed by a joint analysis of METEOSAT thermal-infrared images and SSM/I data, the first used to discriminate clouds and the latter employed to identify possible precipitation within the cloud system. The data processing has consisted in applying an unsupervised clustering algorithm in order to group the METEOSAT thermal-infared pixels, colocated within SSM/I ones, into four classes: clear sky, low, medium, and high clouds. Then, the scattering index (SI) has been computed from SSM/I data [3]. Limiting the discussion to land surface only, SI is empirically defined by the following equation [3]:

$$\mathrm{SI} = 451.9 - 0.44T_B(19_v) - 1.775T_B(22_v) + 0.005\,75T_B(22_v)^2 - T_B(85_v) \quad (8)$$

$T_B(f_p)$ being the brightness temperature at frequency f and polarization p (v for vertical, h for horizontal). By producing the monthly histograms of SI values belonging to the clear-sky class (according to METEOSAT), we have inferred the SI threshold that is able to detect pixels without precipitation and to account for the intrinsic variability of the surface. The SI threshold has been considered equal to $\mathrm{mode}_{\mathrm{SI}} + 2\sigma_{\mathrm{SI}}$, where $\mathrm{mode}_{\mathrm{SI}}$ is the modal value, and σ_{SI} is the standard deviation of SI estimated from the clear-sky histogram. The factor two has been assumed in order to guarantee a conservative choice.

In Fig. 3, the clear-sky histograms of SI are compared with those referring to other METEOSAT classes (i.e., low, medium, and high clouds). The SI threshold is indicated by an arrow in the figure. Values above the threshold, denoting the presence of clouds and rain, are particularly associated with medium and high clouds, thus supporting the rationale of the implemented procedure. Note that in this way we have implicitly adapted the SI threshold to the area of interest and have accounted for its annual variability. Following these results, the evaluation of surface emissivity from (7) has been carried out only for either METEOSAT clear-sky zones or METEOSAT cloudy pixels with SI below the chosen threshold.

The radiative variables T_{mrUP}, T_{mrDN}, and τ in (7) have been estimated, for each SSM/I pixel, by running the radiative-transfer model using as input the meteorological vertical profiles provided by the National Center for Environmental Prediction and the National Center for Atmospheric Research (NCEP/NCAR). The NCEP/NCAR data are available all over the earth's surface, with a spatial resolution of 2.5° both in longitude and in latitude and with a number of vertical layers equal to 17, starting from the height corresponding to an atmospheric pressure of 1000 mbar. Therefore, a vertical interpolation/extrapolation of profiles has been performed to the surface values according to the surface elevation in the SSM/I pixel, derived by a low-resolution digital elevation model (DEM). Furthermore, a horizontal interpolation has been necessary because of the different spatial resolution and location between SSM/I pixels and NCEP data.

As for the horizontal interpolation, T_{mrUP}, T_{mrDN}, τ, and T_s at each SSM/I pixel location have been computed by a bilinear interpolation taking into account the four NCEP grid points surrounding the pixel. As a test, we have verified that, with respect to nearest neighbor interpolation, the maximum difference in emissivity is below 0.017 for low-resolution channels and 0.07 for the 85-GHz channel. The vertical extrapolation/interpolation at the surface of the NCEP temperature profiles has been performed by applying a linear fitting to the NCEP temperatures within the troposphere for adiabatic profiles, or interpolation of the lower two values in case of inversions (i.e., depending on

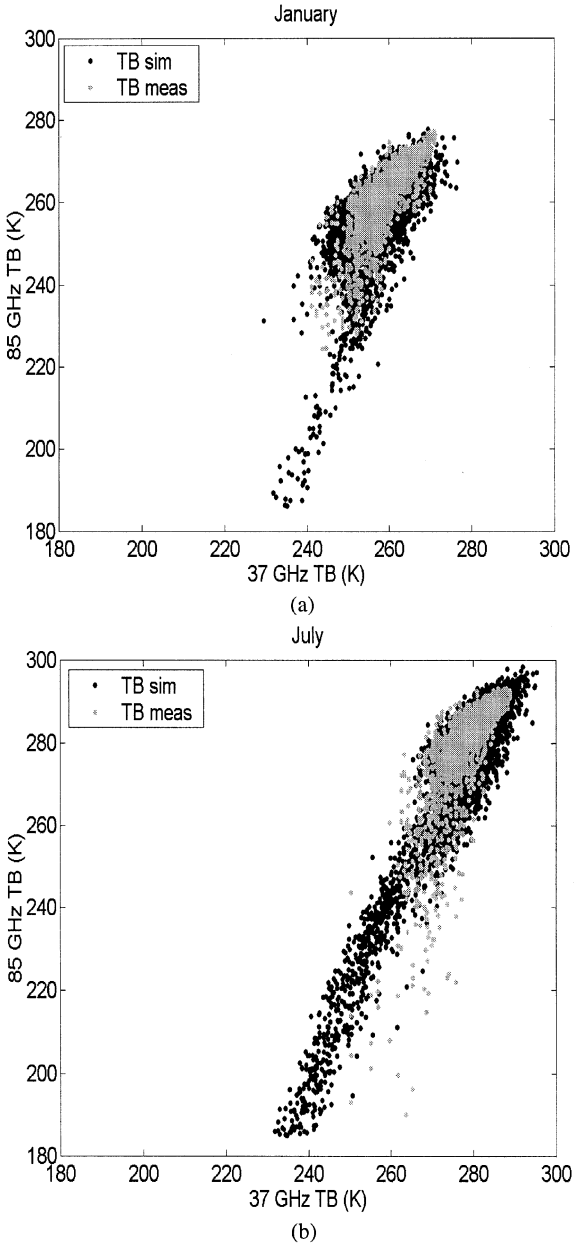

Fig. 6. Comparison between final simulations and SSM/I measurements of T_B at 37 and 85 GHz over central Italy for (a) January 1995 and (b) July 1995.

the atmospheric stability condition). Regarding the pressure, we have performed an exponential fitting of the lower three levels, while the surface humidity has been equated to that at the lowest NCEP level. Note that the interpolation/extrapolation height for each SSM/I pixel is derived by reading the DEM. To assess the accuracy of such interpolation/extrapolation, we have applied it to RAOB profiles disregarding the surface values. By comparing the results with respect to all the RAOB profiles, the maximum differences between truth and estimated values for τ and T_s were about 0.01 and 1 K, respectively.

Fig. 4 presents two maps of mean emissivity at 85 GHz (horizontal polarization), derived for January and October 1995. The variation of emissivity from January to October in the Alpine region due to the snow cover in winter can be clearly observed. When computing the emissivity mean vector and covariance matrix, only unpolarized emissivity over land has been

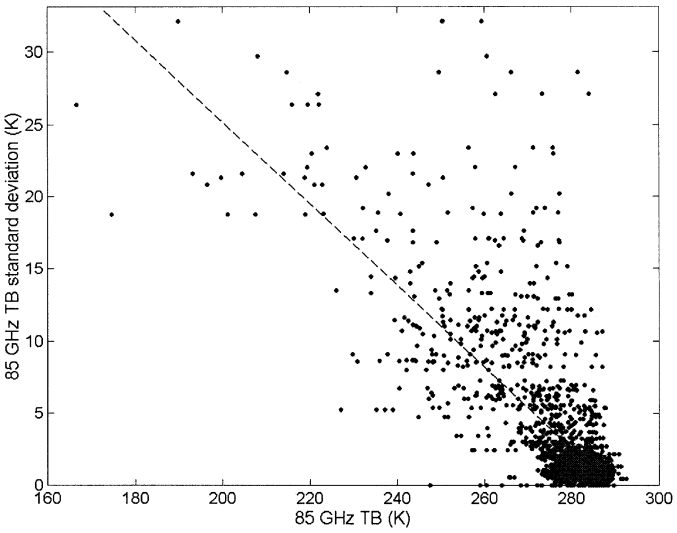

Fig. 7. Scatterplot of the *inhomogeneity index* of the 85-GHz channel inside the low-resolution 37-GHz field of view as a function of the 85-GHz T_B. The best fitting line is also indicated.

considered by averaging vertical and horizontal channels, since polarization signature over land has been demonstrated not to be relevant [19]. Fig. 5 summarizes the result of this analysis, showing plots of annual variation of mean values and standard deviations of the unpolarized surface emissivity in the inland of central Italy (see Section III) at 19 and 85 GHz. The high spatial and temporal variability of surface emissivity, shown by previous figures, has been incorporated in the simulations in order to account for its high uncertainty in the retrieval process.

As previously mentioned, the adopted radiative-transfer model assumes a plane-parallel geometry for characterizing each cloud structure. The gaseous absorption has been determined by means of the Liebe model [21], as in [19]. The hydrometeors have been supposed to be spherical and described by an inverse-exponential size distribution parameterized to hydrometeor content and surface rainfall rate [17].

Fig. 6 shows the results of the physical–statistical matching process in terms of comparison between T_B values simulated and measured by SSM/I over central Italy at 37 and 85 GHz, both for winter (January) and for summer (July) conditions over land. An overall comment is that T_B values belonging to the cloud-radiative synthetic database tend to reproduce SSM/I measurement domain fairly well. The T_B simulations cover a larger portion of the diagram with respect to the measurements, since the heaviest rain clouds, available in the synthetic database, are rarely detected in the Mediterranean region by SSM/I. It should be pointed out that such a fairly good matching is achieved only by generating different simulated datasets for each month. In other words, the consideration of the annual variation of the statistical parameters used to produce the synthetic cloud structure and their background has revealed itself to be essential.

In Fig. 6(b), related to July 1995, there are some measurements, characterized by very low T_B values at 85 GHz and moderate values at 37 GHz that are not covered by simulations. These T_B points are probably representative of small-scale convective structures typical of the Mediterranean region during

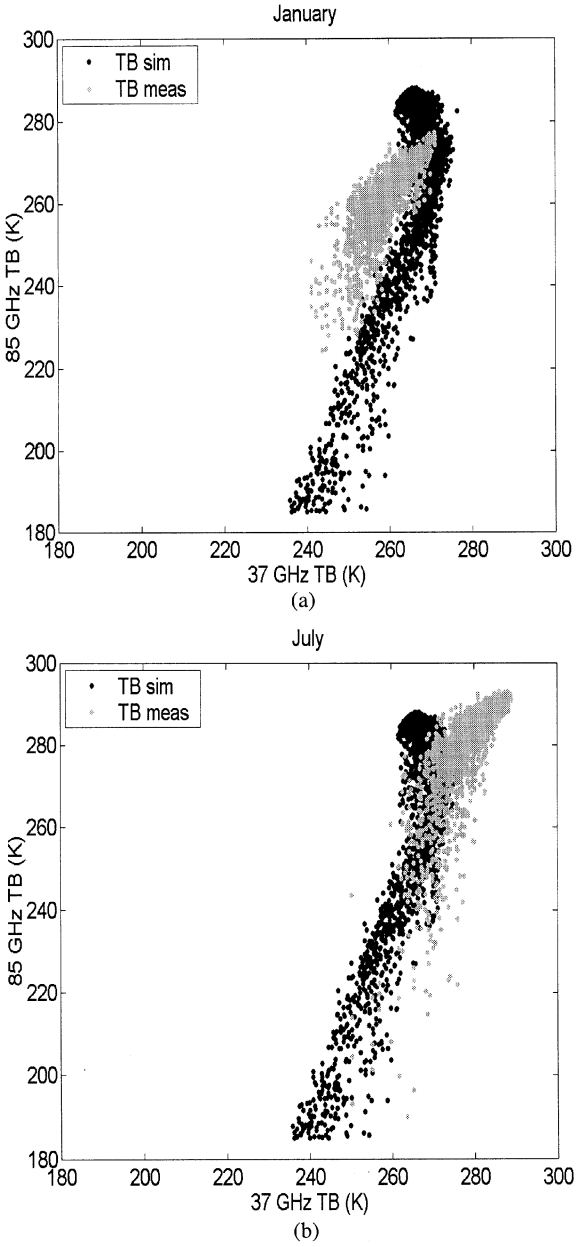

Fig. 8. Comparison between simulations and SSM/I measurements of T_B at 37 and 85 GHz as in Fig. 6, but obtained without applying the matching technique.

summer and autumn. These thunderstorm structures have generally a horizontal extension of a few kilometers, thus being at most detectable by the high-resolution SSM/I channels (i.e., 85 GHz), but not resolved by the low-resolution ones. This issue is known as the beam-filling problem and represents a critical aspect of a physical retrieval procedure assuming plane-parallel cloud structures, since the horizontal inhomogeneity of clouds cannot be taken into account in the training synthetic database.

Several works have dealt with this problem attempting either to detect or to solve it in the retrieval algorithm [22], [23]. Even if this is not an objective of this work, in order to prove the above assumption about the anomalous points in Fig. 6, a very simple cloud T_B *inhomogeneity index* has been introduced as the standard deviation of the 85-GHz T_B values within the low-resolution 37-GHz footprint [24]. A good correlation has been found between this index and the 85-GHz T_B, with low values of the latter corresponding to greater inhomogeneity. Fig. 7 shows the experimental scatterplot between these two quantities, indicating that the highly convective cloud cells (characterized by low 85-GHz T_B values) are usually smaller than the 37-GHz pixel resolution, thus generating the anomalous spectral signatures in Fig. 6. This is a strong indication that the beam-filling problem can be a major cause of some discrepancies between the plane-parallel simulations and spaceborne measurements, particularly in summer.

C. Marginal Role of Various Sources of Constraints

In order to evaluate the marginal role of the various constraints used in the physical–statistical matching described previously, a sensitivity analysis has been carried out.

Fig. 8 shows the same comparison represented in Fig. 6, but before applying the various steps of the physical–statistical matching. The presence of a bias between SSM/I measurements and simulations is clearly observed for lower T_B values. This bias is particularly evident in January and can be explained by considering that the unmatched synthetic database basically relies on a simulation of a summer storm whose geometrical and microphysical properties are not always suitable for use over the Mediterranean area [19]. A comparison between Figs. 6 and 8 puts in evidence the importance of introducing monthly dependent information derived from actual observations in order to obtain a veritable database of synthetic T_B's.

For the sake of evaluating both the marginal contribution of each individual data source and its impact on the overall tuning procedure, we have built the training database by considering the introduction of each source one at a time. Therefore, we have separately imposed progressively the following constraints:

- — profiles of clear air meteorological parameters (from RAOBs) and cloud heights (from RAOBs and METEOSAT);
- — surface emissivity mean and covariance (from SSM/I and METEOSAT data and NCEP analysis);
- — mean profiles of hydrometeor contents (from rain-gauge measurements).

For each $\mathbf{t}_m$ measured by SSM/I over land, within the region depicted in Fig. 4, the closest $\mathbf{t}$ has been searched in the monthly synthetic database by minimizing the Euclidean distance $d = |\mathbf{t}_m - \mathbf{t}|$ in the multifrequency T_B space. Mean value and standard deviation of distance d provide a measure of how well the synthetic database reproduces the SSM/I measurement set. These results are reported in Table I, together with rain retrieval errors that will be discussed in Section III. The combined use of both meteorological parameters and emissivity estimates largely enhances the representativeness of the simulated database, while the scaling factor tends to give a smaller improvement to the accuracy of T_B simulations (but it reveals itself essential to improve rain retrievals, as discussed later on). The matching of meteorological profiles, based on RAOB data, will not significantly decrease the distance d if it is not coupled with the estimation of the surface emissivity statistics. The same conclusion can be drawn if only the information about surface emissivity is introduced.

TABLE I
CONTRIBUTION OF THE VARIOUS SOURCES OF REFERENCE DATA TO IMPROVE BOTH THE MATCHING OF DATABASE T_B'S WITH MEASUREMENTS AND THE RAIN RATE RETRIEVALS (EACH LINE INCLUDES ONE MORE SOURCE, STARTING FROM THE UNMATCHED DATABASE). FIRST TWO COLUMNS ARE MEANS AND STANDARD DEVIATIONS OF DISTANCE BETWEEN T_B MEASURED BY SSM/I AND THE CLOSEST T_B IN THE DATABASE. LAST THREE COLUMNS COMPARE THE RAIN RATES ESTIMATED FROM SSM/I AT BASIN LEVEL WITH THOSE MEASURED BY THE RAIN-GAUGE NETWORK BY REPORTING ERROR BIAS, ERROR STANDARD DEVIATION, AND CORRELATION COEFFICIENT, RESPECTIVELY

	T_B distance mean	T_B distance stand. dev.	RR comparison correlation	RR estimate error bias	RR estimate error stand. dev.
Without matching	10.00	5.12	0.33	-0.55	1.34
With RAOB's data	13.74	5.98	0.36	-1.51	2.66
With emiss. data	11.43	5.03	0.36	-1.08	1.71
With RAOB's & emiss. data	1.12	0.87	0.58	-0.13	0.53
matched database	1.10	0.63	0.68	-0.03	0.37

III. RETRIEVAL RESULTS

The maximum *a posteriori* probability (MAP) criterion can be used to classify cloud genera and to estimate the gross profile of hydrometeor contents and related surface rain rate, using a single- or two-step approach. The details of the MAP technique are illustrated in [14] and [15], while in [19] an analysis of the expected classification accuracy is reported.

To shortly resume the single-step algorithm, given a vector of measured brightness temperature $\mathbf{t}_m$ (multifrequency and eventually multipolarization), the most probable profile $\mathbf{g}_i$ of a cloud belonging to class i is inferred by searching in the database the cloud class i and profile $\mathbf{g}_i$ that minimize the following functional:

$$d(\mathbf{t}_m, \mathbf{g}_i) = [\mathbf{t}_m - \mathbf{t}(\mathbf{g}_i)]^T \mathbf{C}_\varepsilon^{-1} [\mathbf{t}_m - \mathbf{t}(\mathbf{g}_i)] + \ln[\det(\mathbf{C}_\varepsilon)] + (\mathbf{g}_i - \mathbf{m}_i)^T \mathbf{C}_i^{-1} (\mathbf{g}_i - \mathbf{m}_i) + \ln[\det(\mathbf{C}_i)] + D\ln(2\pi) \quad (9)$$

where $\mathbf{t}(\mathbf{g}_i)$ is the modeled T_B vector (associated with the cloud vector $\mathbf{g}_i$ in the training synthetic database); $\mathbf{C}_\varepsilon$ is the covariance matrix of the error ε affecting either the measured T_B and the modeled one [15]; $\mathbf{C}_i$ is the covariance matrix of the $\mathbf{g}$ vectors within class i; $\det(\cdot)$ indicates the determinant; superscripts "T" and "-1" indicate transposition and inversion of a matrix, respectively.

SSM/I estimates of rain rate have been compared with rain-gauge measurements over the Tiber River basin available every 30 min. For each rain-gauge site, the closest SSM/I measurement has been identified for both high-resolution and low-resolution channels, and the rain-gauge cumulated precipitation has been converted to rain intensity in millimeters per hour. The maximum accepted distance between rain-gauge location and 85-GHz pixel center has been assumed equal to 7 km. When several rain gauges have fallen within one SSM/I pixel, their precipitation intensities have been averaged. SSM/I pixels labeled as coastlines have been disregarded, while those close to these coastline pixels have also been included only if their clear-air temporal trend at 19 GHz was within an expected range of variability (note that SSM/I 19-GHz channel has a field of view of about 60 km). It has been already pointed out in the previous section that, due to the rain-gauges time sampling of 30 min, an error of ± 15 min in the time correspondence between data may exist, together with possible

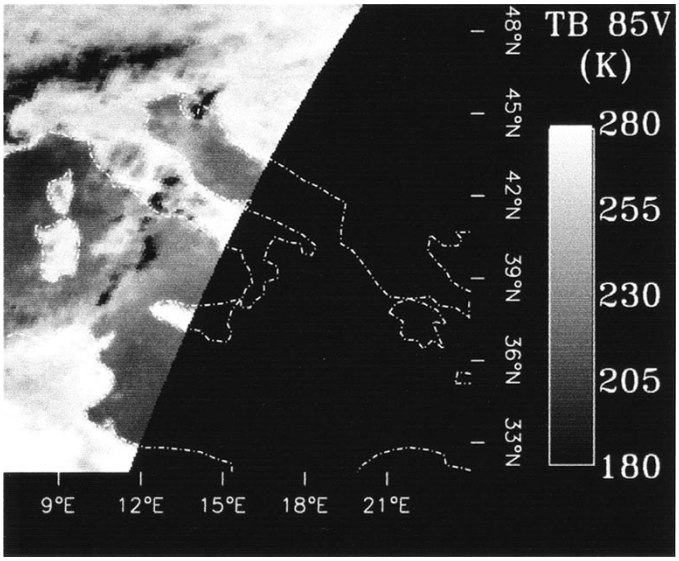

(a)

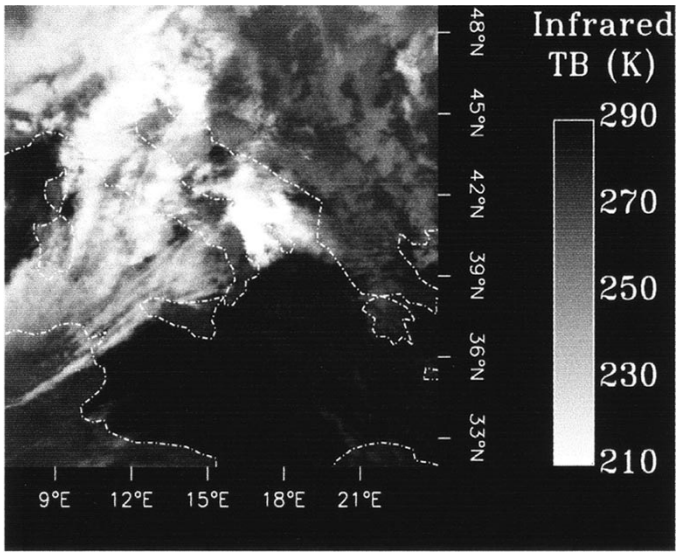

(b)

Fig. 9. (a) SSM/I image at 85 GHz, vertical polarization, acquired on March 4, 1995 at 0616 UTC (white corresponds to higher T_B) and (b) the corresponding infrared METEOSAT image available at 0630 UTC (white corresponds to low temperature). Note that the SSM/I swath covers only part of the geographical box.

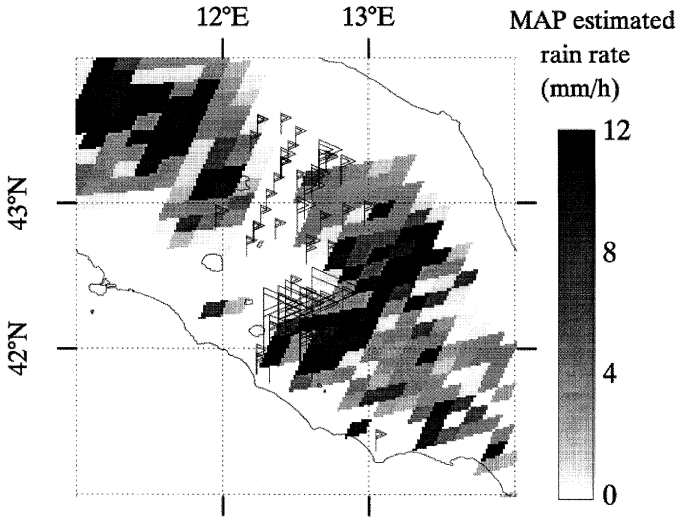

Fig. 10. Rain rate estimated by SSM/I represented as a grayscale map, compared to rain rates measured by each rain gauge. Rain-gauge locations are indicated by flags, whose height gives the measured rain intensity (in the range 0–12 mm/h). Smallest flags stand for operating rain gauges that did not detect rain.

SSM/I geolocation errors. Moreover, the intercomparison has to take into consideration the different spatial and temporal integrations of the two instruments together with possible undetected contaminations from coastline radiometric signatures.

A. Analysis of Case Studies

The analysis of some case studies can help to understand and discuss the SSM/I capability to retrieve rain, as well as the problems encountered during the validation step. For this reason, we have chosen both a successful example of SSM/I retrievals and also one of the worst cases encountered in the comparison work.

An example of a mid-latitude mesoscale cloud system over central Italy is presented in Fig. 9, which shows the SSM/I image at 85 GHz at vertical polarization, acquired on March 4, 1995 at 0616 UTC (white color in the image corresponds to higher T_B) and the corresponding infrared METEOSAT image available at 0630 UTC (white corresponds to low temperature). From METEOSAT, it emerges that cloud coverage extends from northern Africa to the northern coast of the Adriatic Sea, with cold areas down to 215 K over central Italy, probably due to either convective cells or ice clouds. This ambiguity is fairly well explained by SSM/I data, whose signature is closely related to liquid-water emission and precipitating-ice scattering. Over the Tiber River valley in central Italy (at about 42° N, 12.5° E) two dark spots with 85-GHz T_B's of about 210 K suggest the impact of cloud convection, while a gray area over Tuscany (a region in central Italy to the north of the Tiber River valley, at about 43.5° N, 1.5° E) indicates less microwave scattering effects, even though with cloud-top infrared temperatures similar to the mentioned dark spots. It is noticeable that a band between these two areas, mostly corresponding to Umbria (another region in central Italy that lies along the Tiber River valley to the south of Tuscany), is covered by clouds with higher top temperatures (according to METEOSAT), but with 85-GHz T_B values comparable to cloud-free ones.

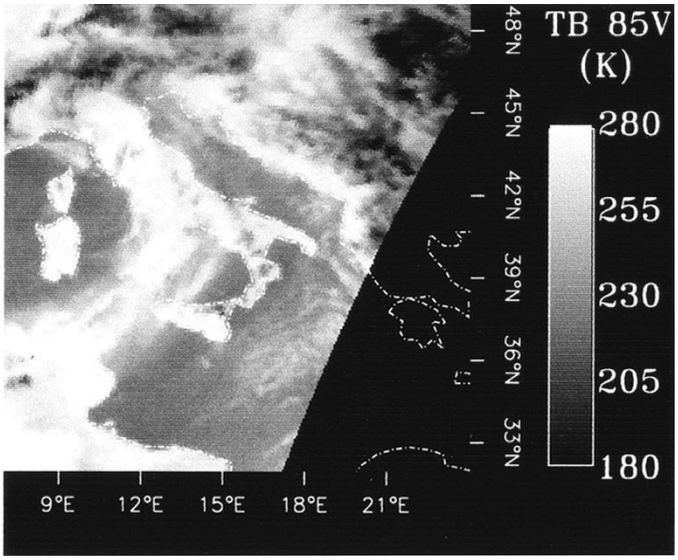

(a)

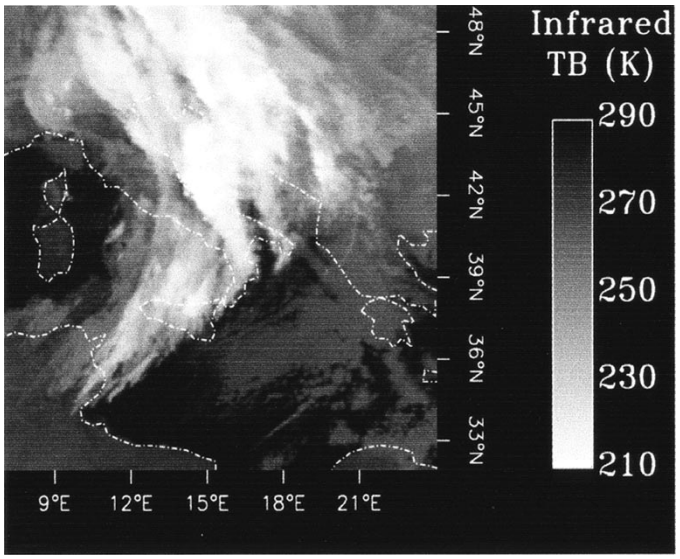

(b)

Fig. 11. (a) SSM/I image at 85 GHz, vertical polarization, acquired on January 19, 1995 at 0551 UTC (white corresponds to higher T_B) and (b) the corresponding infrared METEOSAT image available at 0600 UTC (white corresponds to low temperature). Note that the SSM/I swath covers only part of the geographical box.

Fig. 10 shows the comparison between rain rates measured by the rain-gauge network and the MAP estimates derived from SSM/I. The flags indicate the presence of an operating rain gauge, while their height is proportional to the measured rain rate, spanning a range of values from 0–12 mm/h. Note that it has been chosen to represent the presence of a rain gauge with the smallest flag, even in absence of detected rainfall.

Most high rain rate values, measured by rain gauges, agree with the SSM/I estimates and are mainly related to depression of the 85-GHz T_B (note the pixels around 42° N, 12.5° E). A discrepancy seems to occur in the mentioned band over Umbria, where the estimated rain rate is zero as opposed to moderate rain (flags of middle height) detected by rain gauges. This error may

be interpreted as due to the presence of shallow clouds with high water content but low precipitating ice, i.e., cloud structures that have a radiometric signature not easily detected over land.

An example of a large discrepancy between rain-gauge and SSM/I data is represented by image acquisition on January 19, 1995 at 0551 UTC. This is a case that has originated one of the worst comparisons, with strong underestimation of SSM/I rain retrievals with respect to rain-gauge measurements. Fig. 11 shows both the METEOSAT cloud-top temperature at 0600 UTC and the 85-GHz radiometric image at vertical polarization. Analogously to Fig. 9, Fig. 12 shows the comparison between rain rates, measured by rain gauges and spanning values from 0–4 mm/h and the corresponding ones from SSM/I pixels.

It is apparent from Fig. 12 that rain is not detected by SSM/I where it is revealed by rain gauges. METEOSAT seems to indicate that over the Tiber River basin the cloud system is in the decaying phase of its evolution. Relatively low cloud cover with high water content tends to produce a moderate rain rate that SSM/I is not capable of detecting because of the low radiative contrast with respect to the uncovered surface signature. On the contrary, rain clouds seems to be well sensed by SSM/I over the Tyrrheanian Sea, as they appear very bright in the 85-GHz image compared to the uncovered sea. Higher clouds are detected by METEOSAT over the Adriatic Sea, but they are not associated to convective systems according to SSM/I. This could indicate that SSM/I has correctly recognized they are formed by ice clouds that do not affect the 85-GHz channels sensibly and are not producing precipitations. Unfortunately, reference data are not available in that area for comparison.

B. Statistical Validation Using Rain-Gauge Data

A quantitative comparison using all passes of the F11-DMSP platform over central Italy has been carried out. The results, referring to the comparison of measurements at a pixel level (e.g., estimates from SSM/I against colocated rain-gauge data), have been found to be fairly scattered, as expected considering all the temporal and spatial mismatching problems mentioned above [25], [26]. The correlation coefficient between estimates and rain-gauge data was about 0.51 with an error standard deviation of 2.3 mm/h. This is aligned with the results from other comparison works using rain gauges and radars [2], [3].

In order to compensate for the different mentioned problems, the comparison has been carried out by spatially averaging both SSM/I and rain-gauge data over the Tiber River basin, i.e., by comparing precipitation data at the basin level. The comparison at the basin level is presented in Fig. 13, which shows rain rates estimated by the MAP algorithm applied to SSM/I data as a function of the rain-gauge values, both averaged over the Tiber River basin. The correlation coefficient between rain gauge and rain rates derived from SSM/I is about 0.68 with an error standard deviation of 0.37 mm/h and a bias of -0.03 mm/h. In this case, the residual dispersion of data points is probably due to the inherent problems of overland radiometric retrieval and different time/space integrations of the two sources of data, more than space mismatching. However, the results can be considered encouraging when compared to those obtained by applying other algorithms proposed in literature to our validation set. For example, the algorithm proposed in [3] for global-scale retrievals has resulted in a correlation coefficient of 0.61, a standard deviation of 0.45 mm/h, and a bias of -0.08 mm/h.

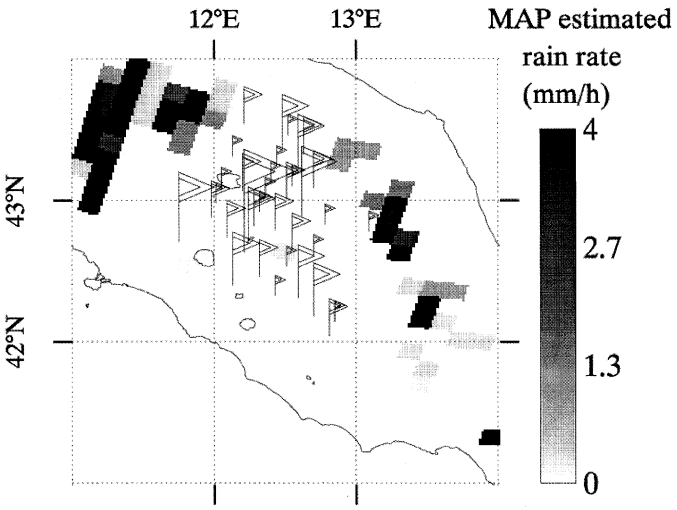

Fig. 12. Rain rates estimated by SSM/I represented as a grayscale map, compared to rain rates measured by each rain gauge. Rain-gauge locations are indicated by flags, whose height gives the measured rain intensity (in the range 0–4 mm/h). Smallest flags stand for operating rain gauges that did not detect rain.

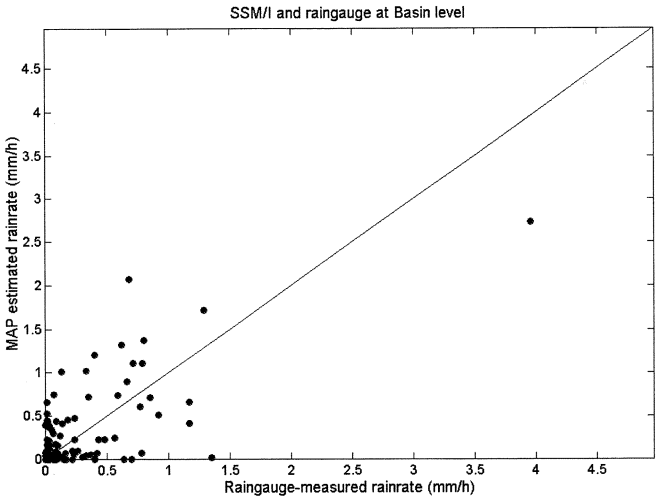

Fig. 13. Comparison between SSM/I estimates of rain-rate and rain-gauge measurements over central Italy at the basin level.

Some of the worst comparisons, observed in Fig. 13, correspond to situations similar to the second case study presented in Section II-A. A relevant result of the proposed hybrid approach, based on the model matching procedure, is that it gives rise to a very small bias at a basin level (about -0.03 mm/h). As for the pixel-level analysis (not shown), it emerges that the rain-gauge observations, characterized by high intensity, are often underestimated by SSM/I. This underestimation does not play a major role in the retrieval at a basin level, and it may be due in many cases to the presence of small and isolated convective cells that are smoothed away by the low SSM/I spatial resolution.

A deeper analysis of the role of this work on SSM/I rain retrieval results has been carried out by quantitatively consid-

ering the marginal role of each source of constraint considered when generating the training database. Columns 3–5 of Table I show the results in terms of rain rate retrieval accuracy, obtained by using progressively each source of constraint, as explained in Section II-C. Again, as already seen in Section II-C, a significant improvement is achieved when both meteorological constraints from RAOB and surface emissivity statistics are introduced. This time the scaling of hydrometeor water contents has also revealed itself to be important to improve the comparison. Note that, thanks to the physical–statistical matching, the correlation between surface precipitation estimates and rain-gauge measurements has been improved by about a factor of two with respect to the same quantity obtained without any matching (i.e., 0.68 versus 0.33), while the bias has been reduced by a factor even bigger than ten (i.e., -0.03 versus -0.55).

IV. Conclusion

Since physical–statistical approaches to retrieve precipitating cloud parameters from spaceborne microwave radiometric data generally start from the availability of a training database, the need for matching such databases to the climatological conditions of the area of interest has been emphasized in this work. In order to carry out this analysis, climatological constraints have been derived on a monthly basis from available radiosounding profiles, rain-gauge network measurements, SSM/I data, and colocated METEOSAT infrared measurements. These constraints have complemented the numerical simulation outputs, provided by a mesoscale cloud-resolving model that is able to explain the microphysics of clouds. The proposed approach can be generalized to other climatic areas when similar reference data were available. The need for considering the annual variability of the climatological constraints has also been demonstrated.

A validation has been performed by comparing both SSM/I observations with brightness temperature simulations belonging to the synthetic database and rain rate retrievals from SSM/I with rain rates measured by a rain-gauge network along the Tiber River basin in Italy. The achieved radiometric representativeness of the modeled databases can be reputed fairly satisfactory, being clusters of measured points well superimposed to database points. As for the rain-gauge comparison, it has been shown that, after the physical–statistical matching step, the rain rates from SSM/I and rain gauges, both averaged within the Tiber River basin, do not exhibit any bias. The comparison has shown a fairly good overall correlation with few relevant discrepancies. From the analysis of these cases, it has emerged that these discrepancies may be due either to inhomogeneity of the observed clouds within the area of interest or to moderate precipitation produced by low shallow clouds.

Acknowledgment

Rain-gauge data have been provided by the Dipartimento per i Servizi Tecnici Nazionali (Rome, Italy). SSM/I data have been provided by NOAA/NESDIS and NOAA/FNMOC. METEOSAT images have been provided by EUMETSAT. We would like to thank the reviewers for their profitable suggestions and comments.

References

[1] R. A. Houze, "Structures of atmospheric precipitation systems: A global survey," *Radio Sci.*, vol. 16, pp. 671–689, 1981.

[2] M. D. Conner and G. W. Petty, "Validation and intercomparison of SSM/I rain-rate retrieval methods over the continental United States," *J. Appl. Meteorol.*, vol. 37, pp. 679–700, 1998.

[3] R. R. Ferraro and G. F. Marks, "The development of SSM/I rain-rate retrieval algorithms using ground-based radar measurements," *J. Atmos. Ocean. Technol.*, vol. 12, pp. 755–772, 1995.

[4] E. A. Smith, A. Mugnai, H. J. Cooper, G. J. Tripoli, and X. Xiang, "Foundations for statistical-physical precipitation retrieval from passive microwave satellite measurements. Part I: Brightness-temperature properties of a time-dependent cloud-radiation model," *J. Appl. Meteorol.*, vol. 31, pp. 506–531, 1992.

[5] C. D. Kummerow, W. S. Olson, and L. Giglio, "A simplified scheme for obtaining precipitation and vertical hydrometeor profiles from passive microwave sensors," *IEEE Trans. Geosci. Remote Sensing*, vol. 34, pp. 1213–1232, Sept. 1996.

[6] P. Hollinger, J. L. Peirce, and G. A. Poe, "SSM/I instrument evaluation," *IEEE Trans. Geosci. Remote Sensing*, vol. 28, pp. 781–790, Nov. 1989.

[7] C. Kummerow, W. Barnes, T. Kozu, J. Shiue, and J. Simpson, "The Tropical Rainfall Measuring Mission (TRMM) sensor package," *J. Atmos. Ocean. Technol.*, vol. 15, pp. 809–817, 1998.

[8] A. Mugnai, E. A. Smith, and G. J. Tripoli, "Foundations for statistical-physical precipitation retrieval from passive microwave satellite measurements. Part II: Emission source and generalized weighting function properties of a time-dependent cloud-radiation model," *J. Appl. Meteorol.*, vol. 32, pp. 17–39, 1993.

[9] F. S. Marzano, A. Mugnai, E. A. Smith, X. Xiang, J. Turk, and J. Vivekanandan, "Active and passive remote sensing of precipitating storms during CaPE. Part II: Intercomparison of precipitation retrievals from AMPR radiometer and CP-2 radar," *J. Meteorol. Atmos. Phys.*, vol. 54, pp. 29–51, 1994.

[10] F. S. Marzano, J. Turk, P. Ciotti, S. Di Michele, and N. Pierdicca, "Potential of combined spaceborne microwave and infrared radiometry for near real-time rainfall attenuation monitoring along earth-satellite links," *Int. J. Satell. Commun.*, vol. 19, no. 4, pp. 385–412, 2001.

[11] P. Bauer and P. Schluessel, "Rainfall, total water, ice water and water vapor over the sea from polarized microwave simulations and SSM/I data," *J. Geophys. Res.*, vol. 98, no. D11, pp. 737–759, 1993.

[12] G. M. Skofronick-Jackson and A. J. Gasiewski, "Nonlinear statistical precipitation retrievals using simulated passive microwave imagery," *IEEE Trans. Geosci. Remote Sensing*, vol. 33, pp. 957–970, July 1995.

[13] K. F. Evans, J. Turk, J. Wong, and T. L. Stephens, "A Bayesian approach to microwave precipitation profile retrieval," *J. Appl. Meteorol.*, vol. 34, pp. 260–279, 1995.

[14] N. Pierdicca, F. S. Marzano, G. d'Auria, P. Basili, P. Ciotti, and A. Mugnai, "Precipitation retrieval from spaceborne microwave radiometers using maximum a posteriori probability estimation," *IEEE Trans. Geosci. Remote Sensing*, vol. 34, pp. 831–846, July 1996.

[15] F. S. Marzano, A. Mugnai, G. Panegrossi, N. Pierdicca, E. A. Smith, and J. Turk, "Bayesian estimation of precipitating cloud parameters from combined measurements of spaceborne microwave radiometer and radar," *IEEE Trans. Geosci. Remote Sensing*, vol. 37, pp. 596–613, Jan. 1999.

[16] G. W. Petty, "The status of satellite-based rainfall estimation over land," *Rem. Sens. Environ.*, vol. 51, pp. 125–137, 1995.

[17] G. Panegrossi, S. Dietrich, F. S. Marzano, A. Mugnai, E. A. Smith, X. Xiang, G. J. Tripoli, P. K. Wang, and J. P. V. Poiares Baptista, "Use of cloud model microphysics for passive microwave-based precipitation retrieval: Significance of consistency between model and measurement manifolds," *J. Atmos. Sci.*, vol. 55, pp. 1644–1673, 1998.

[18] J. H. Christensen, B. Machenhauer, R. G. Jones, R. C. Schär, P. M. Ruti, M. Castro, and G. Visconti, "Validation of present day regional climate simulation over Europe, LAM simulation with observed boundary condition," *Clim. Dynam.*, vol. 13, pp. 489–506, 1997.

[19] G. d'Auria, F. S. Marzano, N. Pierdicca, R. Pinna Nossai, P. Basili, and P. Ciotti, "Remotely sensing cloud properties from microwave radiometric observations by using a modeled cloud data base," *Radio Sci.*, vol. 33, pp. 369–392, 1998.

[20] C. Prigent, W. B. Rossow, and E. Matthews, "Global maps of microwave land surface emissivities: Potential for land surface characterization," *Radio Sci.*, vol. 33, pp. 745–752, 1998.
[21] H. Liebe, "MPM—An atmospheric millimeter-wave propagation model," *Int. J. IR MM Wave*, vol. 10, pp. 631–650, 1989.
[22] C. Kummerow, "Beamfilling errors in passive microwave rainfall retrievals," *J. Appl. Meteorol.*, vol. 37, pp. 356–370, Apr. 1998.
[23] B. Z. Petrenko, "The beamfilling algorithm for retrieval of hydrometeor profile parameters from passive microwave measurements," *IEEE Trans. Geosci. Remote Sensing*, vol. 39, pp. 117–124, Jan. 2001.
[24] Y. C. Hong, C. D. Kummerow, and W. S. Olson, "Separation of convective and stratiform precipitation using microwave brightness temperature," *J. Appl. Meteorol.*, vol. 38, pp. 1195–1213, 1999.
[25] N. Pierdicca, G. d'Auria, L. Pulvirenti, P. Basili, S. Bonafoni, P. Ciotti, and F. S. Marzano, "Validation of rain measurements by spaceborne microwave radiometry using a raingage network in the Tiber basin," in *Proc. IGARSS*, Boston, MA, July 2000, pp. 1–3.
[26] L. Pulvirenti, P. Castracane, G. d'Auria, N. Pierdicca, and F. S. Marzano, "A physical-statistical approach to match spaceborne microwave radiometric retrieval of rainfall to Mediterranean climatology," in *Proc. IGARSS*, Sydney, Australia, July 9–13, 2001.

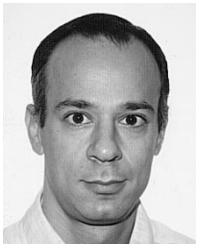

Luca Pulvirenti received the Laurea degree in electronic engineering from the University "La Sapienza," Rome, Italy, in 1999, where he is currently pursuing the Ph.D. degree in applied electromagnetics and electrophysics sciences.

His research interests include microwave remote sensing of atmosphere and earth surface and is presently focused on microwave radiometry of cloudy systems.

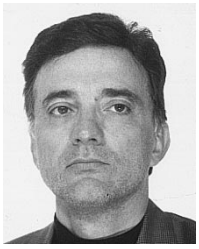

Nazzareno Pierdicca was born in Rome, Italy, on June 11, 1954. He received the Laurea (Doctor's) degree in electronic engineering *(cum laude)* from the University "La Sapienza," Rome, Italy, in 1981.

He is currently an Associate Professor in the Faculty of Engineering of the University "La Sapienza" and teaches remote sensing and antennas. From 1978 to 1982, he was with the Italian Agency for Alternative Energy (ENEA), performing research and development activities in the field of thermal and mechanical behavior of the nuclear fuel rod. From 1982 to 1990, he worked with Telespazio, Rome, in the Remote Sensing Division. He was involved in and responsible for various projects concerning remote sensing applications, data interpretation, and ground segment design. He was Principal Investigator of the ESA/JRC Agrisar'86 airborne campaign and Co-Investigator of the X-SAR/SIR-C experiment. In November 1990, he joined the Department of Electronic Engineering at the University "La Sapienza." His research interests mainly concern electromagnetic scattering models, microwave radiometry of the atmosphere, and SAR land applications. He has been Investigator of the MAC Europe'91 and X-SAR/SIR-C experiments.

Frank Silvio Marzano (S'89–M'99) received the Laurea degree *(cum laude)* in electrical engineering (1988) and the Ph.D. degree (1993) in applied electromagnetics both from the University "La Sapienza," Rome, Italy.

He currently teaches a course on antennas and propagation and coordinates the satellite and radar remote sensing group within the Center of Excellence (CETEMPS) in the Department of Electrical Engineering, University of L'Aquila, L'Aquila, Italy. In 1993, he collaborated with the Institute of Atmospheric Physics (CNR), Rome, Italy. From 1994 till 1996, he was with the Italian Space Agency, Rome, Italy, as a Post-Doctorate Researcher. After being a Lecturer at the University of Perugia, Perugia, Italy, in 1997 he joined the Department of Electrical Engineering, University of L'Aquila. His current research interests are passive and active remote sensing of the atmosphere from ground-based, airborne, and spaceborne platforms, with a particular focus on precipitation using microwave and infrared data, development of inversion methods, radiative-transfer modeling of scattering media, and scintillation and rain-fading analysis along satellite microwave links.

Dr. Marzano received the Young Scientist Award of the XXIV General Assembly of the International Union of Radio Science in 1993. In 1998, he was the recipient of the Alan Berman Publication Award from the Naval Research Laboratory, Washington, DC.

Paolo Castracane was born in Rome, Italy, on January 23, 1971. He received the Laurea degree in physics (1996) and the Ph.D. degree in the field of remote sensing of the lower atmosphere (2000), both at the University of Rome "La Sapienza," Rome, Italy.

Presently he holds a Post-Doctorate position in the Department of Electronic Engineering, University of Rome "La Sapienza." His research interests are mainly electromagnetic scattering models, microwave radiometry of the atmosphere, SAR land applications, and planetary boundary layer meteorology.

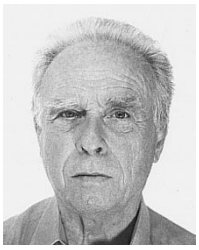

Giovanni d'Auria was born in Rome, Italy, on June 23, 1931. He received the degree in electrical engineering and the Libera Docenza degree from the University of Rome "La Sapienza," Rome, Italy, in 1956 and 1964, respectively.

He served in the Italian Air Force, working in the ITAV Laboratories. He was then with Fondazione Ugo Bordoni as Researcher in the Antennas and Propagation Laboratory. He joined the Department of Electronics, University of Rome "La Sapienza," in 1962 as an Assistant Professor, teaching applied electronics. In 1976, he was appointed Professor in the Chair of Antennas and Propagation and has been teaching this subject ever since. His current research interests are EM propagation in a turbulent atmosphere, microwave remote sensing of the atmosphere and earth's surface, and microwave radiometry of the atmosphere, particularly of cloud systems.